This article has been accepted for inclusion in a future issue of this journal. Content is final as presented, with the exception of pagination.

Predicting the Radiated Emissions of Automotive Systems According to CISPR 25 Using Current Scan Methods

Jin Jia, Denis Rinas, and Stephan Frei, *Senior Member, IEEE*

***Abstract*—According to automotive standard CISPR 25, electronic components or modules are required to be connected to a specific test cable bundle in order to evaluate the radiated emissions. In the absorber-lined shielded enclosure (ALSE) method, also called the antenna method, the cable bundle is often the dominant radiation structure due to its length. This measurement method requires a large anechoic chamber, but often, it is only the impact of the test cable bundle's common-mode (CM) current distribution that is measured. Since the current distribution can be measured easily with current clamps, and with much lower demands to the environment, it is advantageous that the level of radiated fields can be estimated from the measured current distribution. This paper presents a field prediction method, which combines a measured CM current distribution with numerical computations for the radiated fields in the frequency range of 30–1000 MHz. Applicability is discussed based on several complex test cases. Three major problems had to be solved. First, appropriate current phase measurement methods had to be developed since the current amplitudes are not sufficient for estimating the electric fields. Second, a CM radiation model of a cable bundle had to be found. Third, in order to get comparable data for the ALSE test environment, a method had to be developed that could take this influence into account. Different solution approaches are examined here for the problems mentioned above.**

***Index Terms*—Absorber-lined shielded enclosure method, antenna method, cable bundle, common-mode current, CISPR 25, phase measurement, radiated emission.**

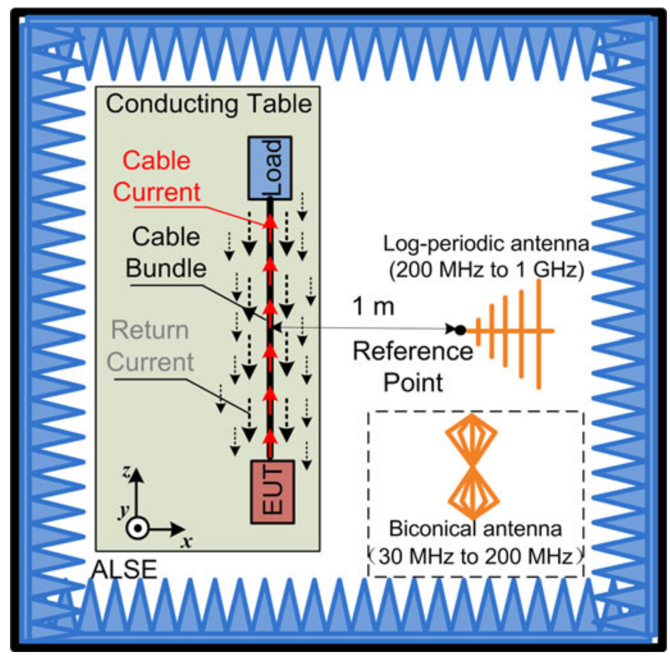

Fig. 1. Simplified radiated emissions test configuration via ALSE method from 30 MHz to 1 GHz.

I. Introduction

The absorber-lined shielded enclosure (ALSE) method from CISPR 25 [1] for measuring the radiated emissions of a system is often assumed to show the best correlation to the device emission behavior in a complete vehicle. In this method, the equipment under test (EUT) is connected to peripheral devices and the supply through a cable bundle of about 1.5 m, as shown in Fig. 1. The radiated fields from this configuration are measured with a biconical, or log-periodic, antenna in the frequency range of 30 MHz to 1 GHz. To eliminate extraneous disturbances and to avoid wall reflections, this method requires an anechoic shielded chamber, which means there will be a higher cost and greater space consumption. During a new product's development, especially when a device repeatedly fails to meet specifications, ALSE measurements might significantly increase the cost of development. Therefore, improved measurement methods are desirable not only for reproducing the ALSE method but also for providing additional analysis information on the root cause of the disturbances.

In many cases, the radiated fields of a cable bundle are dominated by the common-mode (CM) current. The radiation of the terminating printed circuit boards (PCBs) can often be neglected due to short structures, especially at lower frequencies. CM current measurements, combined with the field calculations, can be seen as an alternative to direct field measurements.

Different approaches regarding CM current distribution-based field estimations were published in the past. One approach is based on a transfer function between the measured CM currents and the antenna voltage [2]–[4]. For radiation, the essential phase shift along the cable bundle was only roughly approximated by an empirically derived function [2], which would lead to serious inaccuracies, especially at high frequencies. In [3], the transfer function method was applied to an electrical

Manuscript received June 22, 2015; revised November 11, 2015; accepted December 14, 2015.

J. Jia was with the On-board Systems Laboratory, TU Dortmund University, Dortmund 44227, Germany. He is now with the China Automotive Engineering Research Institute (CAERI), Chongqing 401122, China (e-mail: jin.jia@tu-dortmund.de).

D. Rinas and S. Frei are with the On-board Systems Laboratory, TU Dortmund University, Dortmund 44227, Germany (e-mail: denis.rinas@tu-dortmund.de; stephan.frei@tu-dortmund.de).

Color versions of one or more of the figures in this paper are available online at http://ieeexplore.ieee.org.

Digital Object Identifier 10.1109/TEMC.2015.2511185

drive system, but only for frequencies below 30 MHz. When the frequency goes above 30 MHz, the accuracy of the transfer function method is low [4]. Another transfer function can be found on a surface around the test setup using the near-field distribution and the test antenna voltage [5]. This approach was developed for simplifying the radiation simulation in the large-scale ALSE setup, but it was not applied to complex electronic systems yet. In [6] and [7], equivalent circuit models were developed to simulate the current distribution on the power supply cable bundle and further evaluate its radiated emissions. However, this approach needs accurate EUT circuit models, which are very difficult to find. Furthermore, the equivalent circuit and the lumped parameter approaches tend to be inaccurate at higher frequencies. Other approaches are based on complex numerical models. In [8] and [9], the complex model of a multiconductor transmission line (MTL) was reduced to a simplified MTL model. This requires detailed knowledge of the MTL's geometric parameter set and termination impedances, which is often not available.

In order to realize a CM current-based field prediction for complex applications without knowledge of EUT details or termination conditions in the frequency range of 30 MHz to 1 GHz, three challenges have to be faced: accurate CM current amplitude and phase distribution measurements must be developed, flexible and easily adjustable CM cable models have to be found, and simple radiation models need to be created to consider the real test environment of the CISPR 25 ALSE method. For example, there are reflections caused by the imperfect absorbing materials on the chamber walls. In Section II, frequency and time-domain current measurement methods are proposed. In Section III, electric dipole-based radiation models for a cable bundle over the metallic table are presented. In Section IV, to integrate the real ALSE test environmental factors, a simple calibration method is introduced. In Section V, a twisted pair cable system and a stepper motor drive system are shown as verification examples. In Section VI, the current scan methods' limitations for predicting radiated emissions are discussed. Finally, the performance of the proposed current scan method is summarized in Section VII.

II. Methods for the CM Current Distribution Measurement on Cable Bundles

Determining the CM current distribution on a typical automotive cable bundle requires overcoming two obstacles. First, current amplitudes of critical noise sources can be small and close to the noise level of the measurement equipment. Second, the current's phase distribution must be found. In [10], the phase is measured directly using a vector network analyzer (VNA) or a spectrum analyzer with a phase shifter and several measurements. The necessary amplitude and phase can also be provided via time-domain measurement using an oscilloscope (OS) and applying an FFT [11]. Unfortunately, internal disturbances of the OS limit the accuracy. Neither method is able to provide the required EMC-detector values directly. Both require a reference signal, which can be difficult to find.

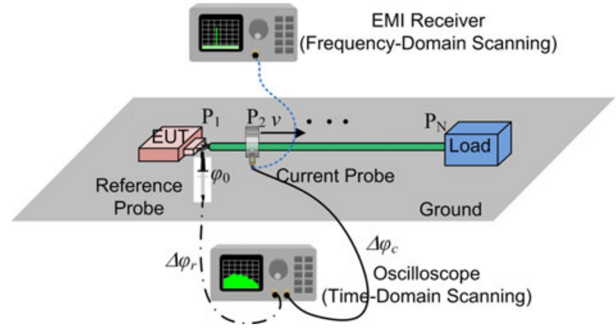

Fig. 2. Basic configuration of the CM current measurement methods with the frequency and time-domain equipment.

In this paper, a method for retrieving the phase distribution, based solely on the measured current amplitude, is introduced and compared to the other approaches. Fig. 2 shows the configuration of the CM current measurement method with the frequency and time-domain equipment.

A. Current Phase Retrieval Based on Spatial Current Amplitude Distribution

The new method for phase retrieval, based on the current amplitude distribution, is described here. This method is based on a CM current substitution model of the bundle and an optimization algorithm for finding the appropriate transmission line (TL) parameters for the substitution model.

The amplitude data-based phase-retrieving algorithm applies TL theory to find an appropriate TL parameter set that can reproduce the amplitude distribution. The current phase distribution can be calculated from this TL model. For this purpose, a CM transmission line model of the cable bundle is needed. In theory, many multiconductor transmission lines can be decoupled to a set of single transmission lines with different modal properties (propagation constants and characteristic impedances) [12]. The modal quantities travel along the modal TLs with different propagation constants and characteristic impedances. The CM mainly propagates between the cable bundle and the ground plate where the air has a lower permittivity than the cable isolation. CM propagation is linked to a propagation speed close to the velocity of light, due to the large distance between the cable bundle and the ground. Other differential modes (DM) mainly propagate between the wires in the cable bundle where the velocities are reduced by the isolation material ($\varepsilon_r > 1$). If a cable bundle consists of tightly packed wires, it is reasonable to neglect the contribution of the DM currents in the radiated emissions if the field observation point's distance is large enough. Therefore, the cable bundle can be simplified to a single wire substitution model with the CM current flowing, as shown in Fig. 3.

For further consideration, the bundle is approximated to a single TL with the measured CM current distribution. The spatial current distribution $I_{\mathrm{com}}(z)$ along a single TL can be expressed by [13]

$$I_{\mathrm{com}}(z) = \left(\frac{e^{\gamma(L-z)}}{1-\Gamma_2}\right)\left(1-\Gamma_2 e^{-2\gamma(L-z)}\right) I_{\mathrm{com}}(L) \quad (1)$$

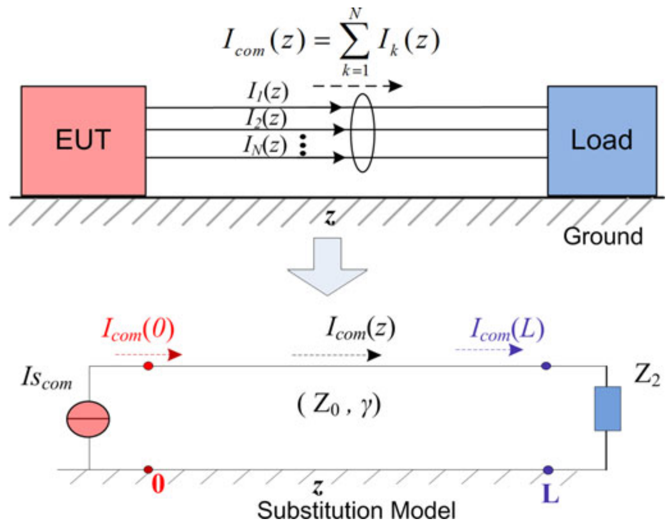

Fig. 3. Multiconductor transmission line and its substitution model for the CM current path.

where $I_{\mathrm{com}}(L)$ is the current at the end of the cable bundle, Γ_2 is the load reflection coefficient defined in (2), and γ is the propagation constant of the cable bundle defined in (3)

$$\Gamma_2 = \frac{Z_2 - Z_0}{Z_2 + Z_0} = A + jB \tag{2}$$

$$\gamma = \alpha + j\beta \tag{3}$$

where Z_0 and Z_2 are, respectively, the characteristic impedance of the TL and the load impedance in the substitution TL model. From (1) to (3), current $I_{\mathrm{com}}(z)$ is a function of the unknown frequency-dependent parameters *A, B,* α, and β. The set of parameters *A, B,* α, and β in (2) and (3) can be found by applying the fitting algorithms to search for the best matches to the measured current amplitude distribution. Before applying the fitting algorithm, the current distribution expression (1) is transformed into a quadratic normalized function

$$\boldsymbol{F}(z) = \left|\frac{I_{\mathrm{com}}(z)}{I_{\mathrm{com}}(L)}\right|^2 = \left|\left(\frac{e^{\gamma(L-z)}}{1-\Gamma_2}\right)\left(1-\Gamma_2 e^{-2\gamma(L-z)}\right)\right|^2. \tag{4}$$

Substituting (2) and (3) into (4), $\boldsymbol{F}(z)$ can also be expressed in terms of *A*, *B*, α, and β

$$\boldsymbol{F}(z) = \left|\left(\frac{e^{(\alpha+j\beta)(L-z)}}{1-(A+jB)}\right)\left(1-(A+jB)e^{-2(\alpha+j\beta)(L-z)}\right)\right|^2 \tag{5}$$

where $\boldsymbol{F}(z)$ is a nonlinear function, where the position coordinates along cable bundle z and $\boldsymbol{F}(z)$ are known, but parameters *A*, *B*, α, and β still need to be found. By measuring the noisy current amplitude distribution at the scanning points, an equation for every current measurement point is found. The overdetermined equation system needs a suitable optimization method to search for the best matching parameter set. The trust-region-reflective (TRR) iterative algorithm [14] was found to be suitable for this problem. The objective function *S* is expressed by

$$\begin{aligned} S &= \min \|\boldsymbol{F}(\alpha,\beta,A,B,z) - \boldsymbol{F}_{\mathrm{meas}}(z)\|_2^2 \\ &= \sum_{i=0}^{m} [\boldsymbol{F}(\alpha,\beta,A,B,z_i) - \boldsymbol{F}_{\mathrm{meas}}(z_i)]^2. \end{aligned} \tag{6}$$

Due to the very small values of the attenuation constant α for automotive cables (α can be approximated by $R/(2Z_0)$ [15]), the losses can be neglected, and α can be set to zero. This leads to a better convergence of the fitting algorithm. Moreover, the characteristic impedance Z_0 of the cable bundle can be estimated from the simple analytic formulas for a bare wire above ground. To reduce the search boundary of the fitting algorithm, the load impedance Z_2 can be evaluated by (7) first, which is based on the maximum and minimum positions of the CM current's amplitude distribution [16]. In (7), *m* is the ratio of the amplitude's minimum to the maximum, and $L_{\min}$ is the distance of the nearest amplitude minimum to the end of the cable bundle. In this case, the load reflection coefficient Γ_2 can be calculated from the fitting algorithm, and the load impedance Z_2 can be furthermore calculated by (8)

$$Z_2 = Z_0 \frac{1/m - j\tan(\beta L_{\min})}{1 - j(1/m)\tan(\beta L_{\min})}, \quad m = \frac{\min(I_{\mathrm{com}}(z))}{\max(I_{\mathrm{com}}(z))} \tag{7}$$

$$Z_2 = Z_0 \frac{1+\Gamma_2}{1-\Gamma_2}. \tag{8}$$

Aside from the search boundaries in the TRR algorithm, suitable initial search conditions are also required. $A = B = \alpha = 0$ and $\beta = 2\pi f / c_0$ are used here to start the parameter search, with c_0 as the velocity of light in a vacuum, and *f* is the considered frequency. After the possible parameters *A, B,* α, and β are found at each frequency, the phase distribution of the CM current on the cable bundle can be retrieved using (1). The advantage of the phase retrieval algorithm is that it only needs the spatial CM current's amplitude distribution along the cable bundle.

B. Current Phase Reconstruction Based on FFT from the Time-Domain Current's Data

By using the time-domain measurement data from an OS and applying the FFT algorithm, the amplitude and phase over the frequency can be obtained directly. This method can be applied as an alternative to the phaseless amplitude measurements. A reference signal is required to receive the phase difference between the different scanning points. The current at the starting point of the cable bundle can be used as a reference for triggering the OS at each location along the cable, always at the same slopes of the repetitive signal, which is a prerequisite for most scanning methods. In practice, this signal can be very weak and a direct voltage measurement on a cable or at the PCB might be necessary for acquiring stable trigger events. The relative phase distribution can be calculated according to (9). Here, φ_N is the current phase at the *N*th position P_N as shown in Fig. 2; φ_0 is the phase from the reference signal; and $\Delta\varphi_r$ and $\Delta\varphi_C$ are the phase shifts caused by the cables from the reference probe and the current probe connected to the OS, respectively. The cable

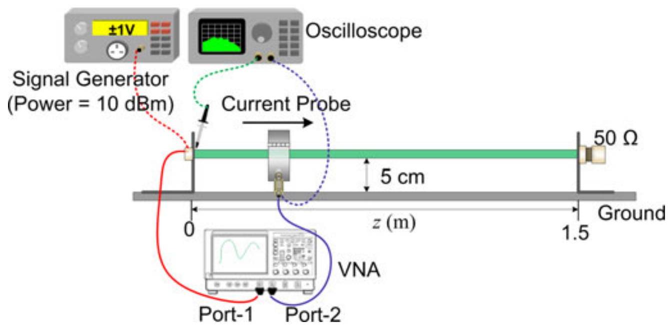

Fig. 4. Wire current distribution acquisition by a VNA or an OS.

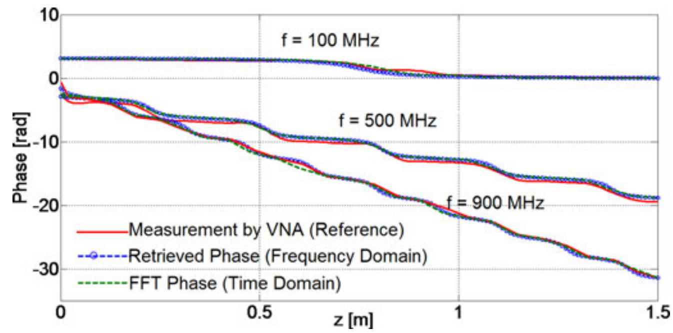

Fig. 5. Current phase distribution from direct VNA measurement, from the retrieval algorithm (amplitude-only from VNA as input) and from FFT from scope measurement data in time domain.

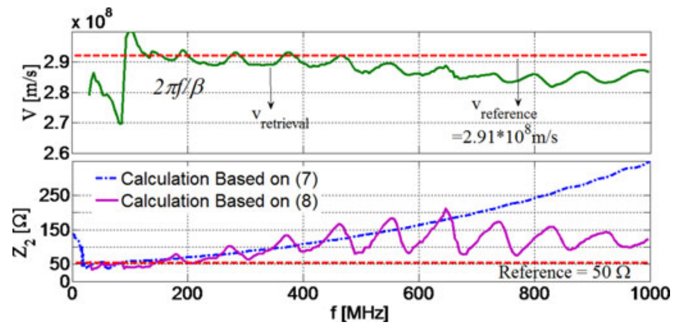

Fig. 6. Retrieved TL parameters based on current amplitude data.

phase shifts can be removed by normalizing the phase at each position to the cable end position according to (10).

$$\begin{aligned}
&\mathbf{P_1}: [\varphi_1 + \Delta\varphi_c] - [\varphi_0 + \Delta\varphi_r] = [\varphi_1 - \varphi_0] + [\Delta\varphi_c - \Delta\varphi_r] \\
&\mathbf{P_2}: [\varphi_2 + \Delta\varphi_c] - [\varphi_0 + \Delta\varphi_r] = [\varphi_2 - \varphi_0] + [\Delta\varphi_c - \Delta\varphi_r] \\
&\qquad\qquad\vdots \qquad\qquad\qquad\qquad \vdots \\
&\mathbf{P_N}: [\varphi_N + \Delta\varphi_c] - [\varphi_0 + \Delta\varphi_r] \\
&= [\varphi_N - \varphi_0] + [\Delta\varphi_c - \Delta\varphi_r]
\end{aligned} \tag{9}$$

$$\begin{aligned}
&\mathbf{P_1 P_N}: \varphi_1' = [\varphi_1 - \varphi_N] \\
&\mathbf{P_2 P_N}: \varphi_2' = [\varphi_2 - \varphi_N] \\
&\qquad\vdots \\
&\mathbf{P_N P_N}: \varphi_N' = 0.
\end{aligned} \tag{10}$$

C. Estimation of the Accuracy of Real Current Scan Data

In order to validate these phase computation methods, a 1.5-m-long isolated single wire was driven by a VNA (Agilent E5071B), and the current's amplitude and phase were measured directly. The wire was terminated by a 50 Ω load. The height of the wire above the ground plane was 5 cm. The wire characteristic impedance was calculated to $Z_0 = 270\ \Omega$, and the propagation velocity ($2\pi f/\beta$) was measured as $v = 2.91 \times 10^8$ m/s. For time-domain investigations, this wire was driven by a battery-supplied signal generator (Signal-Forge 1020) with a sinusoid signal of 10 dBm of power at different frequencies. The currents were measured using an OS (LeCroy Wavepro 7200 A). The voltage at the cable's starting position provides the reference phase for the current's phase distribution calculation. Fig. 4 depicts the basic verification configuration.

Only amplitude data were used during the investigation of the phase-retrieving algorithm from the VNA. The phase distributions—which are retrieved from amplitude data, measured in the frequency domain and calculated using the FFT from the time-domain data—nearly coincide to the directly measured phase from the VNA at the considered frequencies, as shown in Fig. 5. Fig. 6 compares the retrieved wire's TL parameters to the reference values. Some deviations can be observed. Since the retrieved TL parameters mainly reflect the mathematical fitting parameters, they might not reflect the physical case. Due to the existence of measurement errors the TRR iterative algorithm often forces the parameters A, B, α, and β to reach the condition of objective function defined in (6), at the expense of sacrificing their physical meanings. In real applications, doing antenna measurements according to CISPR 25 can require the acquisition of very weak antenna voltages. Especially when class 5 is demanded, the currents causing the radiation can be very low. The limitations of the sensitivity of the measurement equipment have to be considered.

III. Field Calculation From a Current Distribution Over a Finite Metallic Plate

When the CM current distribution $I_{\rm com}(z)$ is available, an appropriate radiation model for the cable bundle and the metallic table is needed. For the calculation of radiated fields from a cable structure, several analytical, e.g. [17]–[19], or numerical approaches are available. In order to save computation, time numerical methods were discarded and a multiple-dipole radiation model was applied here to represent the real cable bundle [20], as shown in Fig. 7.

The cable bundle is divided into N short segments, modeled as radiating Hertzian dipoles. The electromagnetic field, at any point from a single dipole, can be found using formulas from [15]. For example, the y-component field is given by

$$H_y^d = \frac{-IdLx}{4\pi r}\beta_0^2 \left(j\frac{1}{\beta_0 r} + \frac{1}{\beta_0^2 r^2} \right) e^{-j\beta_0 r} \tag{11}$$

This article has been accepted for inclusion in a future issue of this journal. Content is final as presented, with the exception of pagination.

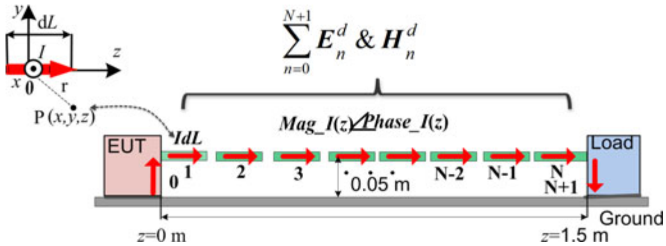

Fig. 7. Multiple-dipole model for the cable bundle in radiation calculation.

$$E_y^d = \frac{IdL \cdot zy}{4\pi r^2}\eta_0\beta_0^2\left(j\frac{1}{\beta_0 r} + \frac{3}{\beta_0^2 r^2} - j\frac{3}{\beta_0^3 r^3}\right)e^{-j\beta_0 r} \tag{12}$$

where r is the distance from the dipole to the observation point P; ε_0 is the dielectric constant of the vacuum; dL is dipole length; I is the current through the modeled segment; η_0 (377 Ω) is the wave impedance in the vacuum; $\beta_0(2\pi/\lambda)$ is the electromagnetic wave phase constant in the vacuum. Radiation from a cable bundle can be calculated by superposition. However, the radiation contribution from EUT and load structure is difficult to determine due to the complex current distribution. If the EUT and load structures are small (i.e., emissions can be ignored) and connected directly to the ground by a wire or the displacement current between the EUT and the ground plate, it is reasonable to model these structures with two vertical connection segments as shown in Fig. 7.

The two assumed connection segments, 0th and $(N + 1)$th, from the cable to the ground, must be considered with additional vertical dipoles in this radiation model [20]. The currents for the vertical connection segments are not known directly from the current measurements but can be found through approximating these by the measured currents at the 1st and Nth segments or by extrapolating with the currents calculated from (1) and using parameters γ and Γ_2 from a calculation with the proposed phase-retrieval algorithm. Afterward, the calculated currents at position $z = -0.025$ m and $z = 1.525$ m are used to represent the 0th and the $(N + 1)$th segment currents, respectively. The extra length of 25 mm for extrapolation refers to the half-length of the connection segments.

A simple equivalent surface current model is applied to model the radiation from the finite ground, as shown in Fig. 8.

The ground plate is modeled with a set of dipoles. The dipole currents can be found from the surface current density $\boldsymbol{J}$ that can be calculated by [21]

$$\begin{aligned}\boldsymbol{J} = {} & J_x\boldsymbol{e}_x + J_z\boldsymbol{e}_z \approx \boldsymbol{e}_n \times (\boldsymbol{H}^{\mathrm{TL}} + \boldsymbol{H}^{\mathrm{TL\_mirror}}) \\ \approx {} & -H_z\boldsymbol{e}_x + H_x\boldsymbol{e}_z\end{aligned} \tag{13}$$

where $\boldsymbol{e}_n(= -\boldsymbol{e}_y)$ is the unit vector normal to the surface, $\boldsymbol{H}^{\mathrm{TL}}$ is the magnetic field from the TL over the ground plate, and $\boldsymbol{H}^{\mathrm{TL\_mirror}}$ is the magnetic field from the mirror image of the TL, according to mirror theory. For each grid element in Fig. 8, the current can be approximately calculated by

$$I_{\mathrm{dip}x}\boldsymbol{e}_x = \Delta L_z \cdot J_x\boldsymbol{e}_x I_{\mathrm{dip}z}\boldsymbol{e}_z = \Delta L_x \cdot J_z\boldsymbol{e}_z. \tag{14}$$

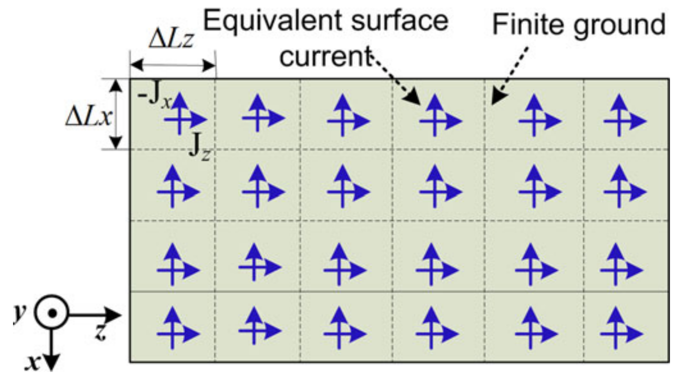

Fig. 8. Replacement of the finite ground plate by a set of equivalent dipoles.

With the radiation formulas of the single dipole model, the total fields can be calculated due to the surface currents using the superposition principle. $I_{\mathrm{dip}x}$ on the plate, for example, produces the y-directional electric field component

$$E_y^P = \sum_{k=1}^{N}\frac{I_{\mathrm{dip}x}^k\Delta L_x^k \cdot (z - z_k)(y - y_k)}{4\pi r_k^2} \times \eta_0\beta_0^2\left(j\frac{1}{\beta_0 r_k} + \frac{3}{\beta_0^2 r_k^2} - j\frac{3}{\beta_0^3 r_k^3}\right)e^{-j\beta_0 r_k} \tag{15}$$

where N is the number of grid elements on the plate, r_k is the distance from the kth grid center (x_k, y_k, z_k) to the observation point (x, y, z), and ΔL_x^k is the kth grid element length in the x-direction. The total radiated field from the cable bundle on the finite ground plate ($\boldsymbol{E}^{\mathrm{Total}}$ and $\boldsymbol{H}^{\mathrm{Total}}$) can be calculated by adding these contributions: the field from the TL in free space ($\boldsymbol{E}^{\mathrm{TL}}$ and $\boldsymbol{H}^{\mathrm{TL}}$) and the scattered field from the TL-induced currents on the ground plate ($\boldsymbol{E}^P$ and $\boldsymbol{H}^P$) according to

$$\boldsymbol{E}^{\mathrm{Total}} = \boldsymbol{E}^{\mathrm{TL}} + \boldsymbol{E}^p \tag{16}$$

$$\boldsymbol{H}^{\mathrm{Total}} = \boldsymbol{H}^{\mathrm{TL}} + \boldsymbol{H}^p. \tag{17}$$

In order to verify the proposed multidipole model for the cable and the surface current model for the finite ground plate, an ALSE configuration, as shown in Fig. 1, was modeled and simulated with an a Method of Moment (MoM) solver [22]. A single wire (see Fig. 4) was driven by a 1 V source with 50 Ω source impedance. Both the finite ground and infinite ground (mirror model) are simulated by MoM. As shown in Fig. 9, the calculated fields from the multidipole model for the wire are in alignment with the MoM fields in the case of the infinite ground plate. The simple surface current model for the finite ground plate is also quite accurate, compared with MoM, except for the horizontal component in the frequency range from 150 to 200 MHz. This deviation is caused by the surface current approximation, which cannot handle edge reflections and resonances.

IV. Considering the ALSE Environment by Calibration

The simple method for field calculation described earlier cannot consider the complex behavior of an anechoic chamber, where the real CISPR 25 measurements are performed. Here

This article has been accepted for inclusion in a future issue of this journal. Content is final as presented, with the exception of pagination.

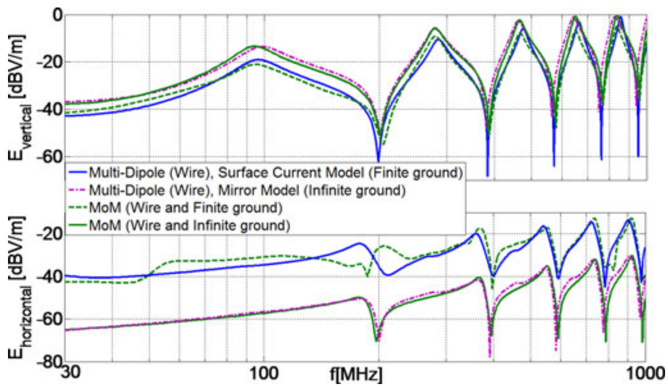

Fig. 9. Vertical and horizontal fields from the wire over a finite ground plate using MoM, surface current model, and mirror model (field observation point is the reference point of the antenna as shown in Fig. 1).

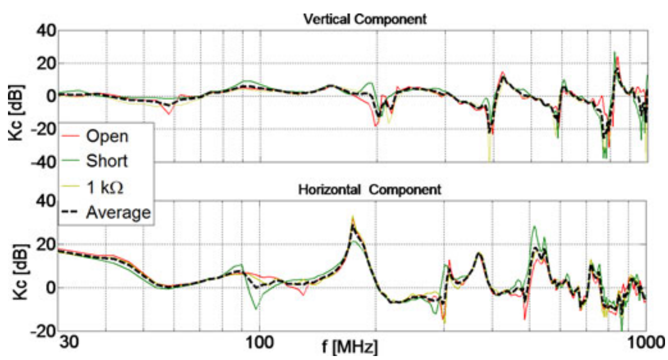

Fig. 10. Correction function of vertical and horizontal polarization.

additional peripheral systems that were not considered in the calculations, reflections from the chamber walls, ALSE ground floor and ground connections from the table to the ALSE wall, or the limited accuracy of the equipment might influence the antenna's voltage. A method for the substitution of ALSE must be able to reproduce a real antenna measurement. Otherwise, such a method will not be accepted. This means that consideration of the problems of this test method is necessary. This can be done by a calibration procedure, as proposed in [23]. In the calibration a single wire of 1.5 m, 5 cm above the ground plate, with 50 Ω source/load impedance is used to obtain a correction function K_c

$$K_c = E_{\rm ac} - E_{\rm am}(\rm dB) \tag{18}$$

where $E_{\rm am}$ is the measured electric field from the test antenna, $E_{\rm ac}$ is the calculated field from the same configuration based on the measured current's distribution. Additionally, several improvements, such as averaging the correction function from different load impedances and preventing radiation from nonwire components, can enhance the match between an antenna's measurement and the proposed method [24]. Fig. 10 shows the vertical and horizontal correction functions when the wire in the calibration configuration is terminated with different load impedances; the source impedance is 50 Ω. The averaged correction function is applied to the example application data in Section V.

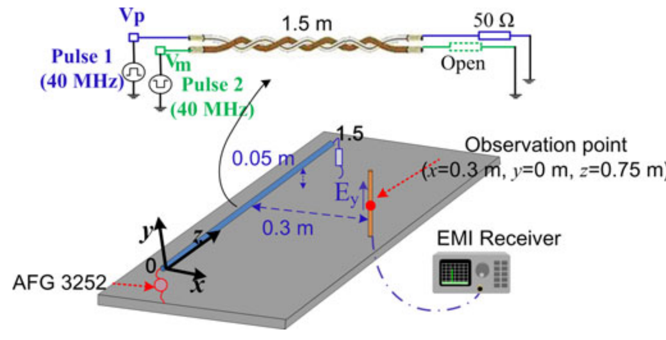

Fig. 11. Twisted-pair cable driven by a differential voltage pair.

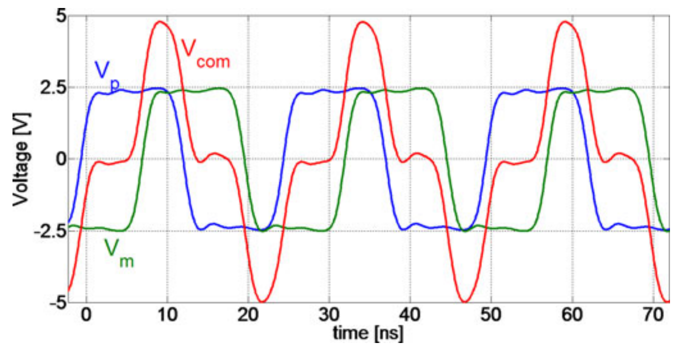

Fig. 12. Differential voltage pair and the resultant CM voltage.

V. Example Applications

In order to validate the presented current scan method, several simple configurations driven by continuous wave signals up to 1 GHz were analyzed in previous works [23], [25]. Two more complex system example investigations are shown here. First, a twisted-pair cable driven by a differential-mode supply is analyzed using a 20 cm calibrated rod antenna to measure the vertical field directly on the metallic table at a distance of 30 cm from the cable. Second, a typical automotive system configuration is investigated. Here a stepper motor is driven by a 16 MHz microcontroller-power-driver-PCB. Only one crystal provides the clock for all PCB systems. A four-wire bundle connects the motor with the PCB. Moreover, a more realistic configuration, according to the CISPR 25, with a Bi-Log antenna is used here at a distance of 1 m from the cable bundle.

A. Twisted-Pair Cable Driven by a Differential Voltage Pair

The wires of the twisted pair configuration were fed by shifted differential trapezoidal voltage pulses from a two-port signal generator (Tektronix AFG 3252), as shown in Fig. 11. One wire was terminated with 50 Ω, and the other was left open. The pulse repetition frequency was 40 MHz. The curve shapes are shown in Fig. 12.

The distance between two measurement points has been chosen according to the shortest wavelength $(\Delta z \sim \lambda_{\min}/10)$. Here, the cable CM currents were each measured at 6 cm. A spline interpolation function gives a continuous current distribution. Current amplitudes are measured using an FCC F-65

This article has been accepted for inclusion in a future issue of this journal. Content is final as presented, with the exception of pagination.

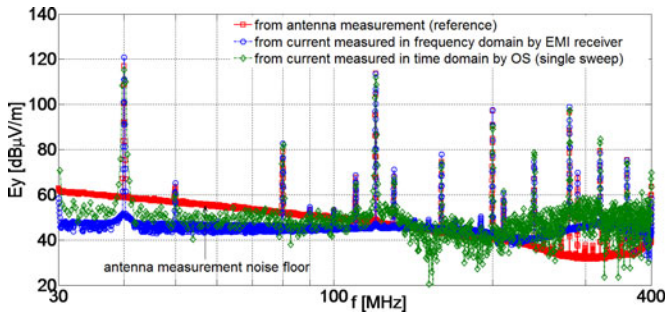

Fig. 13. Electric field from antenna measurement and simulation based on the CM current acquired by the EMI receiver and OS with a single sweep.

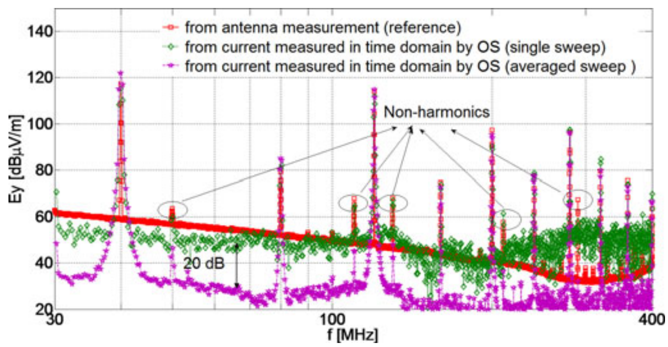

Fig. 14. Electric field from antenna measurement and simulation based on CM current acquired OS with a single sweep and an averaged sweep.

current probe with an EMI receiver [R&S ESPI 3, average detector, 120 kHz bandwidth (BW) and 5 ms measurement time (MT)] or OS (LeCroy Wavepro 7200A, 550 μs sample time and 0.5 ns interval time). Then, phase information at each frequency is calculated using the proposed phase retrieving algorithm or FFT. The phase retrieval algorithm in frequency domain, which is not run-time optimized, needs about 4 min for 9251 frequency points on a 3.3 GHz PC with 8 GB RAM). Finally, the electric field at the observation point is calculated based on a multidipole model for the cable and a mirror model for the ground plate. Without considering the real ALSE test configuration in this example, K_c is not applied here. The antenna measurement is also performed via the EMI receiver with the same settings as those used for the current scan. The antenna is calibrated using a field calculation with Concept II [22]. Fig. 13 shows the electric field of the antenna's measurement and the simulations based on the measured CM currents.

The main radiated frequency peaks include ten harmonics and several nonharmonics (50, 110, 130, 210, and 290 MHz), which might result from the signal generator's control circuit. When compared with the antenna's measurement the calculated deviations at these peaks are less than 4 dB, based on the frequency domain current measured by the EMI receiver. Only the deviation of the component at 400 MHz amounts to 5 dB. When using the time-domain current, measured by the OS, the deviations are less than 6.5 dB in a single sweep. However, the nonharmonic of 290 MHz cannot be recorded by the OS successfully. In Fig. 14, the influence of the averaging function of

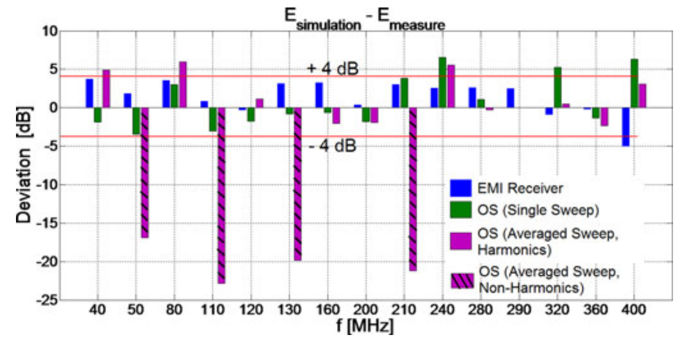

Fig. 15. Field deviation distribution at main frequency peaks from current scan methods by EMI receiver and OS.

the OS is shown. When compared with a single sweep of the OS, the averaged sweep can reduce the noise floor by 20 dB or more and gives nearly the same predicted field value when the amplitude is stable. The large nonharmonic peaks at 50, 110, 130, and 210 MHz might be caused by a nonlinear signal amplification circuit used in the generator. These are much lower due to the use of the averaging function and the nonstable signals. Fig. 15 shows the deviation at the frequency peaks from scanning with the frequency domain and time domain, instead of the direct antenna measurement. Several reasons for these deviations can be identified. First, the common accuracy of the measurement equipment (e.g., ± 2 dB transfer impedance deviation of the used current probe), a scanning position error, and an antenna factor calculation error from the MoM model. Second, the accuracy of the current scanning in the time domain mainly depends on the measurement sensitivity of the OS, the settings, and the FFT algorithm. The sampling frequency, triggering condition, window function, and the average number of sweeps also have a large impact on the data quality.

B. Stepper Motor Drive System

The second investigated configuration (the stepper motor drive system) is shown in Fig. 16, in the anechoic chamber where the reference ALSE antenna measurements were performed. For flexibility in programming, a microcontroller-based board with a 16-MHz clock frequency was used. A 20 dB preamplifier (R&S Hz-16) was added to improve the measurement dynamics.

An EMI receiver (average detector, 120 kHz BW, and 5 ms MT) was used to measure the antenna voltage, which was transferred to the electric field with the antenna factor. The electric fields at the reference point were also calculated based on the cable currents measured by the EMI receiver with the settings from the antenna measurement, or the OS (single sweep, 550 μs sample time, and 0.5 ns sample interval time). The field was calculated by using the multidipole model from Section III. In order to consider the real imperfections of the ALSE test environment, which is far away from the free space environment, the averaged correction function K_c defined in (17) and shown in Fig. 10 is applied.

Figs. 17 and 18 show the predicted fields from the current scan methods and the antenna measurements in the ALSE, for

This article has been accepted for inclusion in a future issue of this journal. Content is final as presented, with the exception of pagination.

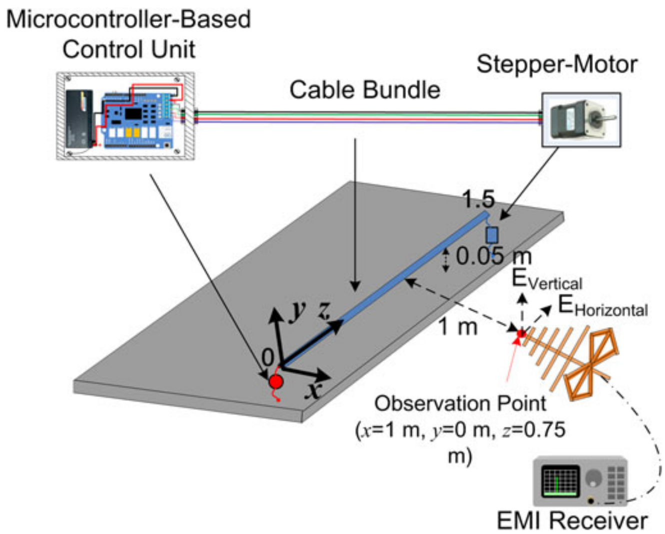

Fig. 16. Test setup of the stepper motor drive system using Bi-Log antenna.

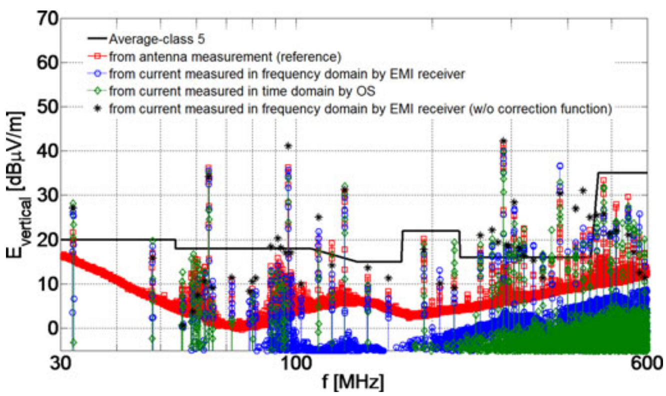

Fig. 17. Vertical electric field from the antenna measurement and simulation based on the cable current acquired by the EMI receiver and OS.

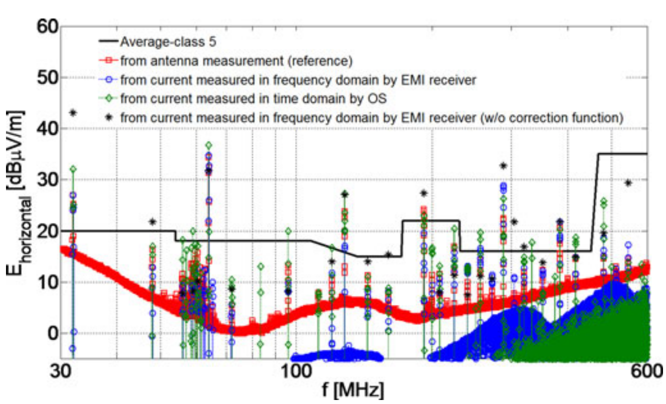

Fig. 18. Horizontal electric field from the antenna measurement and simulation based on the cable current acquired by the EMI receiver and OS.

both the vertical and horizontal polarization up to 600 MHz, where the predicted fields are also shown, without applying the correction function K_c. Radiation above 600 MHz could not be investigated since the signals are very weak and below the limits. The predicted results are very consistent with the measurements

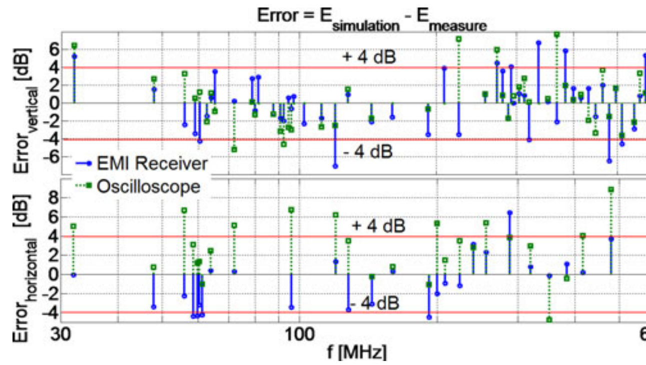

Fig. 19. Vertical and horizontal field deviation distribution at the main frequency peaks from the current scan methods by the EMI receiver and OS.

at the main peaks. The deviations at these peaks are shown in Fig. 19. At the main harmonics peaks in vertical or horizontal polarization, which exceed the limit of the average class-5 (32, 64, 96, 128, 192, 288, and 384 MHz), the errors from the frequency-domain current scanning method using EMI receiver amount to less than 7 dB. The deviations from the time-domain current's scan by the OS are less than 5 dB. These deviations may be caused by the accuracy of the current measurements, the accuracy of the correction function, or the limited accuracy of the measurement equipment.

VI. Discussion

Based on a simple configuration, it could be shown that the accuracy of the current scan methods can be sufficiently high for the precompliance investigations of systems, according to the CISPR 25. Also, for the complex microcontroller–stepper–motor system, useful precompliance data could be gained.

In order to improve the proposed method to predict the radiated emissions of the cable bundles, these three different process steps have to be analyzed: the CM current acquisition on the cable bundle, the field calculation based on the simplified radiation models; and the incorporation of the real ALSE measurement environment through a calibration procedure.

These are the possible error sources for the current acquisition process step:

1) The current amplitude and phase can only be detected with limited accuracy. Phase retrieval methods add a phase error. FFT for the time-domain data is a critical process step that can add significant deviations. The most common distortions due to FFT are described in [26]. The averaging function of the scope increases the dynamic range, but it fails when the signals are not synchronous and change in shape.
2) Calculated fields from current measurements can have a much lower noise floor than direct antenna measurements and might show more details of a disturbing circuit [27].
3) There are inaccuracies in the transfer impedance of the current probe.
4) There are scanning positioning errors. The width of the RF current probe (1.7 cm of the used FCC F-65 probe) may induce resolution errors at high frequencies.

5) The CM current radiation model is only an approximation to reality. The current distribution in the cable bundle wires influences the radiation characteristics.

The field calculation is performed with approximate formulas in order to save computation time. More accurate calculation methods might improve the field prediction quality. The field calculation is done for a single point, the center point of the antenna. However, the voltage given by a real antenna reflects the integration of the field on the whole equivalent antenna area.

Finally, the calibration method for adapting the calculation data to the real measurement environment is based on a sample configuration with more or less arbitrary current and phase distribution along the cable bundle. It cannot be guaranteed that data quality is really improved.

VII. Conclusion

This paper proposes methods to predict radiated emissions from the CISPR-25-compliant ALSE configurations, solely based on the measured current distribution along a cable bundle.

Several problems had to be solved. The most important was to find the spatial current phase distribution along the cable bundle. Two methods were applied here. The first is based on the scanned CM current amplitude data in the frequency domain. The necessary phase information was retrieved by an optimization algorithm, from the current amplitude information. The other method was based on the scanned current data in the time domain, which gives the amplitude and phase information directly via FFT transformation. Here, a reference phase is necessary. When both the CM current amplitude and the phase are available, the electromagnetic fields from the cable bundle can be calculated quickly by a multidipole model. Real ALSE measurement environment influences need to be integrated in the simulation models for the comparison to the direct antenna measurements. In order to reduce the deviations a calibration procedure was introduced to improve the prediction quality.

For validation of the methods, different configurations were analyzed. Radiated emissions from a twisted-pair cable, driven by a differential voltage source, and from a four-wire bundle terminated with a stepper motor and a microcontroller-based motor driver were investigated. It could be shown that the current scan in the frequency domain and the time domain can both predict the radiated emissions from the CM current measurements. This means, at least for the precompliance measurements, that the current scan methods could substitute the ALSE antenna measurements.

References

[1] *CISPR 25: Vehicles, Boats and Internal Combustion Engines-Radio Disturbance Characteristics—Limits and Methods of Measurements for the Protection of On-board Receivers*, IEC, third ed., 2008.

[2] W. T. Smith and K. Frazier, "Prediction of anechoic chamber radiated emissions measurements through use of empirically-derived transfer functions and laboratory common-mode current measurements," in *Proc. IEEE Int. Symp. Electromagn. Compat.*, Aug. 1998, pp. 387–392.

[3] D. Schneider, M. Beltle, B. Siegel, S. Tenbohlen, and W. Kohler, "Radiated emissions of an electric drive system estimated on a bench using disturbance currents and transfer functions," *IEEE Trans. Electromagn. Compat.*, vol. 57, no. 3, pp. 311–321, Mar. 2015.

[4] D. Schneider, M. Bottcher, B. Schoch, and S. Hurst, "Transfer functions and current distribution algorithm for the calculation of radiated emissions of automotive components," in *Proc. EMC Europe*, Brugge, Belgium, Sep. 2013, pp. 443–448.

[5] A. Radchenko, V. V. Khilkevich, N. Bondarenko, D. Pommerenke, M. Gonser, J. Hansen, and C. Keller, "Transfer function method for predicting the emissions in a CISPR-25 test-setup," *IEEE Trans. Electromagn. Compat.*, vol. 56, no. 4, pp. 894–902, Aug. 2014.

[6] G. H. Li, W. Qian, A. Radchenko, and G. Hess, "Estimating the radiated emissions from cables attached to a switching power supply in a MIL-STD 461 test," in *Proc. IEEE Int. Symp. Electromagn. Compat.*, Denver, CO, USA, Aug. 2013, pp. 626–631.

[7] F. Costa, C. Gautier, B. Revol, J. Genoulaz, and B. Demoulin, "Modeling of the near-field electromagnetic radiation of power cables in automotives or aeronautics," *IEEE Trans. Power Electron.*, vol. 28, no. 10, pp. 4580–4593, Oct. 2013.

[8] G. Andrieu, A. Reineix, X. Bunlon, J. P. Parmantier, L. Kone, and B. Demoulin, "Multiconductor reduction technique for modeling common-mode currents on cable bundles at high frequency for automotive applications," *IEEE Trans. Electromagn. Compat.*, vol. 50, no. 1, pp. 175–184, Feb. 2008.

[9] G. Andrieu, A. Reineix, X. Bunlon, J. P. Parmantier, L. Kone, and B. Demoulin, "Extension of the "Equivalent cable bundle method" for modeling electromagnetic emissions of complex cable bundles," *IEEE Trans. Electromagn. Compat.*, vol. 51, no. 1, pp. 108–118, Feb. 2009.

[10] Y. Vives-Gilabert, C. Arcambel, A. Louis, F. De Daran, P. Eudeline, and B. Mazari, "Modeling magnetic radiation of electronic circuits using near-field scanning method," *IEEE Trans. Electromagn. Compat.*, vol. 49, no. 2, pp. 391–400, May 2007.

[11] D. Rinas, S. Niedzwiedz, J. Jia, and S. Frei, "Optimization methods for equivalent source identification and electromagnetic model creation based on near-field measurements," in *Proc. EMC Europe*, York, U.K., Sep. 2011, pp. 298–303.

[12] C. R. Paul, *Analysis of Multiconductor Transmission Lines*. New York, NY, USA: Wiley, 1997.

[13] M. Meyer and P. Asfaux, "Radiated emissions modeling of a power cable," in *Proc. IEEE Int. Symp. Electromagn. Compat.*, Hamburg, Germany, Sep. 2008, pp. 1–5.

[14] *Matlab, Program Documentation, Version R2010a*. Natick, MA: Mathworks Inc., 2010.

[15] C. R. Paul, *Introduction to Electromagnetic Compatibility*. New York, NY, USA: Wiley, 1992.

[16] O. Zinke and H. Brunswig, *Lehrbuch der Hochfrequenztechnik*. New York, NY, USA: Springer, 1986.

[17] R. S. Shi, J. C. Sabonadare, and D. A. Dacherif, "Computation of transient electromagnetic fields radiated by a transmission line: An exact model," *IEEE Trans. Magn.*, vol. 31, no. 4, pp. 2423–2431, Jul. 1995.

[18] J. Jia, F. Kremer, and S. Frei, "Modellierung von CISPR-25 Antennenmessungen mittels schneller approximierender Berechnungsverfahren," presented at the *EMV-Düsseldorf*, Düsseldorf, Germany, 2012.

[19] J. Wang, O. Fujiwara, and K. Sasabe, "A simple method for predicting common-mode radiation from a cable attached to a conducting enclosure," in *Proc. Asia-Pacific Microw. Conf.*, 2001, vol. 3, pp. 1119–1122.

[20] J. Meng, Y. X. Teo, D. W. P. Thomas, and C. Christopoulos, "Fast prediction of transmission line radiated emissions using the Hertzian dipole method and line-end discontinuity models," *IEEE Trans. Electromagn. Compat.*, vol. 56, no. 6, pp. 1295–1303, Dec. 2014.

[21] V. Volski and G. A. E. Vandenbosch, "Efficient physical optics approximation for the calculation of radiation pattern of planar antennas located on a finite ground plane," *IEEE Trans. Electromagn. Compat.*, vol. 53, no. 1, pp. 460–465, Jan. 2005.

[22] CONCEPT-II. *Program information*. (2015). [Online]. Available: http://www.tet.tuhh.de/en/ concept/

[23] J. Jia, D. Rinas, and S. Frei, "An alternative method for measurement of radiated emissions according to CISPR25," in *Proc. EMC Europe*, Brugge, Belgium, Sep. 2013, pp. 2–6.

[24] J. Jia, A. Alexander, D. Rinas, and S. Frei, "Anwendung von alternativen Verfahren zur Vorhersage von EMV Antennenmessergebnissen nach CISPR-25," presented at the *EMV-Düsseldorf*, Düsseldorf, Germany, 2014.

[25] J. Jia, D. Rinas, and S. Frei, "Prediction of radiated fields from cable bundles based on current distribution measurements," in *Proc. EMC Europe*, Rome, Sep. 2012, pp. 1–7.

[26] V. Janssen, "Accelerated EMI measurements with time domain scan," in *Proc. EMC Europe*. Rome: Tutorial, Sep. 2012.

[27] J. Jia, "Current scan methods to predict radiated emissions of automotive components according to CISPR 25," Ph.D. dissertation, Department of Electrical Engineering and Information Technology, TU Dortmund University, Dortmund, Germany, May 2015.

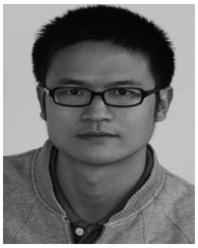

Jin Jia received the Ph.D. degree in electrical engineering from the TU Dortmund University, Dortmund, Germany, in 2015, and the M.S. and B.S. degrees in electrical engineering from Chongqing University, Chongqing, China, in 2010 and 2007, respectively.

He is currently an EMC Engineer in China Automotive Engineering Research Institute (CAERI), Chongqing, China. His current research interests include radiation modeling of complex cable bundles and EMC modeling of automotive electrical and electronic systems.

Denis Rinas received the Diploma in information technology at the TU Dortmund University, Dortmund, Germany, in 2009.

He has been working as a Research Assistant at the On-board Systems Lab, TU Dortmund University. His current research interests include methods to obtain radiation of electronic components, particularly with regard to field-scan methods and modeling for simulation.

Stephan Frei (M'97–SM'13) received the Dipl.-Ing. degree in electrical engineering and the Ph.D. degree from Berlin University of Technology, Berlin, Germany, in 1995 and 1999, respectively.

Between 1995 and 1999, he was a Research Assistant for EMC at the Institute of Electrical Power Engineering, Berlin University of Technology. Between 1999 and 2006, he was with the automobile manufacturer AUDI AG in the Development Department, where he was involved in developing and introducing new methods for the computation of EMC, antennas, and signal integrity in vehicles. Beginning in 2001, he and his team were responsible for the EMC release process of a type series and international standardization. In 2006, he became a Professor for vehicular electronics at TU Dortmund University. He is currently the Dean of the Faculty for Electrical Engineering and Information Technology in Dortmund. His current research interests include EMC, SI, computational methods, and vehicle power supply systems. He is the author or coauthor of more than 150 papers.

Dr. Frei was a Distinguished Lecturer for the IEEE EMC Society from 2008 to 2009.